

Intermingled basins in coupled Lorenz systems

Sabrina Camargo ¹, Ricardo L. Viana ², and Celia Anteneodo ^{1,3}

¹ *Department of Physics, PUC-Rio, Rio de Janeiro, Brazil*

² *Department of Physics, Federal University of Paraná, Curitiba, Brazil*

³ *National Institute of Science and Technology for Complex Systems, Rio de Janeiro, Brazil.*

(Dated: June 3, 2019)

We consider a system of two identical linearly coupled Lorenz oscillators, presenting synchronization of chaotic motion for a specified range of the coupling strength. We verify the existence of global synchronization and antisynchronization attractors with intermingled basins of attraction, such that the basin of one attractor is riddled with holes belonging to the basin of the other attractor and *vice versa*. We investigated this phenomenon by verifying the fulfillment of the mathematical requirements for intermingled basins, and also obtained scaling laws that characterize quantitatively the riddling of both basins for this system.

PACS numbers: 0.45.Xt,05.45.Df,05.45.Pq,05.45.-a

I. INTRODUCTION

Synchronization of periodic oscillations is a long-known phenomenon, described as early as 1665 by Christiaan Huyghens. In a letter to the Royal Society read by Sir Robert Moray in February 27th, 1665; Huyghens reported an “odd kind of sympathy” when two pendulum clocks were suspended by the side of each other [1]. In a letter to his father, Huyghens described this “odd sympathy” as the fact that the pendulum clocks shared a common frequency but were out of phase by π radians. Hence what Huyghens actually saw was antisynchronization of the pendula (as a matter of fact, the observation of Huyghens can be properly classified as phase antisynchronization).

In more recent times, it was discovered that chaotic oscillators, when suitably coupled, can synchronize their trajectories [2]. This phenomenon has been studied for more than two decades, and there is already a wealth of analytical, numerical, and even experimental results on it [3]. For two completely synchronized systems, either periodic or chaotic, their dynamical variables are equal for all times. On the other hand, if two systems antisynchronize, the sum of some of their dynamical variables is zero. Certain dynamical systems with phase-space symmetries can exhibit both synchronized and antisynchronized states, which can be viewed as coexisting chaotic attractors with corresponding basins of attraction, or multistability.

Multistable dynamical systems have typically a very complicated structure of basins of attraction, that may be delimited by fractal boundaries [4]. Such fractality causes a problem with the determination of the final state of the system (i.e., its long-time behavior), once we regard the initial conditions as always having an uncertainty. Let us suppose that the coupled oscillators have two attractors: one related to synchronized and another to antisynchronized behavior, with the corresponding basins of attraction sharing a common basin boundary in the phase space. If a ball centered at a given initial condition and with a radius equal to the uncertainty level intercepts

the basin boundary, we cannot say *a priori* which attractor the system will asymptote to: the final state can be either synchronized or antisynchronized [5].

If the basin boundary is a smooth curve, however, this final-state sensitivity problem can be circumvented by decreasing the radius of the uncertainty ball (this can be done in experimental or numerical settings, by increasing the precision in determining the initial condition in phase space). However, akin reduction of uncertain initial conditions does not occur if the basin boundary is a fractal curve. This problem is more pronounced the more area-filling is the fractal curve. In that limit case, the fraction of uncertain initial conditions will likely not decrease no matter how much we decrease the uncertainty balls of each initial condition.

The latter situation occurs for riddled basins, which can be described as an extreme type of fractal basins, for which the common boundary is a curve practically area-filling, in the sense that the (box-counting) dimension of the basin boundary is close to the dimension of the phase space itself [6]. If riddled basins exist in a multistable chaotic system, their final states are utterly unpredictable, i.e. we cannot say - with any degree of certainty - which attractor the system will evolve to for long times [7]. The situation, in this case, is akin to that for a random process, for which there can only be a given probability for predicting the final state of the system. In fact, some phenomena formerly attributed to random variations in initial conditions can be also interpreted as a consequence of riddling [8]. The simplest case is when only one of the coexisting attractors have a riddled basin. However, there may be cases for which both attractors have riddled basins, and we call the latter intermingled basins.

From the mathematical point of view, riddled basins are observed - under some circumstances - in dynamical systems that exhibit an invariant subspace with a chaotic attractor lying on it, and another asymptotic final state, out of the invariant subspace [9]. For intermingled basins both attractors must lie on invariant subspaces. It turns out that synchronized and antisynchronized states of cou-

pled chaotic oscillators, once they exist, can be represented by attractors lying on invariant subspaces. The remaining conditions for which there can be intermingled basins are related to the stability of these attractors along directions transversal to those subspaces.

The aim of this work is to demonstrate the existence of intermingled basins of attraction for the synchronized and antisynchronized states of two coupled Lorenz oscillators. In a previous work, Kim and coworkers [10] have identified such states and also presented numerical evidence suggesting the existence of a riddled basin of synchronization, but without checking the mathematical conditions for riddling. As a matter of fact, such verification through direct methods (i.e., by making a linear stability analysis of each invariant subspace) is quite difficult in this coupled system, since the phase space is six-dimensional. On the other hand, a one-dimensional reduction of the Lorenz system (to a piecewise approximation to the well-known Lorenz map) was low-dimensional enough for such an analytical treatment to be feasible and show the riddling of the synchronization basin [11]. This result already suggests akin phenomenon for coupled Lorenz systems.

In this paper we pursue another route to characterize quantitatively the existence of riddled basins of attraction: the scaling laws giving the probability of making wrong predictions on the final state of the system, with respect to two parameters of interest: (i) the phase-space distance to the invariant subspace; and (ii) the uncertainty radius for each initial condition [12]. We have verified that, for both parameters, the probability scales as a power-law, as required for riddled basins. Moreover, we compared our numerical results with an analytical theory developed by Ott and co-workers [12], based on the assumption that the dynamics transversely to the invariant subspaces can be governed by a stochastic process with bias and a reflecting barrier. Such treatment was previously applied to other chaotic dynamical systems with a phase-space with large dimensionality [13].

The rest of the paper is organized as follows: Section II describes the coupled system of Lorenz oscillators, as well as the existence of both synchronized and antisynchronized states. Section III presents a preliminary discussion of the basins of attraction of both the synchronized and antisynchronized states. The mathematical properties required for riddled basins and the tools necessary to verify them are the object of Section IV. Section V discusses the quantitative characterization of riddled basins through scaling laws and the theoretical results supporting them. The last Section contains our conclusions and final remarks.

II. COUPLED LORENZ SYSTEMS

The Lorenz system [14]

$$\dot{x} = \alpha(y-x), \quad \dot{y} = \beta x - y - xz, \quad \dot{z} = -\gamma z + xy \quad (1)$$

is one of the paradigmatic nonlinear dynamical systems. Moreover, its equations mimetize the dynamical behavior expected to occur in some physically relevant systems, as convection rolls in the atmosphere [14], single-mode lasers [15], and segmented disk dynamos [16].

For $\alpha = 10$, $\beta = 28$, and $\gamma = 8/3$, there is a chaotic attractor with the familiar butterfly-like shape. The chaotic nature of the dynamics was elegantly suggested by Lorenz, who performed a dimensional reduction by sampling only the local maxima of one of the phase-space variables, so as to get a discrete-time variable, which return map is a unimodal map with a cusp. Since such maps display a similar dynamical behavior as the tent map, this similarity was used by Lorenz to explain the erratic behavior at the chaotic attractor in the three-dimensional phase space.

Many different coupling schemes are possible for two identical Lorenz systems [17]. We have chosen, for symmetry reasons, a diffusive coupling through the z -variable, as follows

$$\begin{aligned} \dot{x}_1 &= \alpha(y_1 - x_1), \\ \dot{y}_1 &= \beta x_1 - y_1 - x_1 z_1, \\ \dot{z}_1 &= -\gamma z_1 + x_1 y_1 + \varepsilon(z_2 - z_1), \\ \dot{x}_2 &= \alpha(y_2 - x_2), \\ \dot{y}_2 &= \beta x_2 - y_2 - x_2 z_2, \\ \dot{z}_2 &= -\gamma z_2 + x_2 y_2 + \varepsilon(z_1 - z_2), \end{aligned} \quad (2)$$

where we will use the same values for α , β , and γ , as in the uncoupled case, and ε is the coupling strength.

On considering the dynamical behavior of the coupled system, it is convenient to perform the changes of variables

$$\begin{aligned} x &= \frac{(x_2 - x_1)}{2}, & y &= \frac{(y_2 - y_1)}{2}, & z &= \frac{(z_2 - z_1)}{2}, \\ X &= \frac{(x_2 + x_1)}{2}, & Y &= \frac{(y_2 + y_1)}{2}, & Z &= \frac{(z_2 + z_1)}{2}, \end{aligned} \quad (3)$$

after which the coupled system (2) becomes

$$\begin{aligned} \dot{x} &= \alpha(y - x), \\ \dot{y} &= \beta x - y - (Xz + Zx), \\ \dot{z} &= -(\gamma + 2\varepsilon)z + Xy + Yx, \\ \dot{X} &= \alpha(Y - X), \\ \dot{Y} &= \beta X - Y - (XZ + xz), \\ \dot{Z} &= -\gamma Z + XY + xy. \end{aligned} \quad (4)$$

We will refer either to the new or the old variables whenever more convenient to the analysis.

From inspecting Eqs. (4) there follows that the dynamics of the coupled system is invariant with respect to the transformation $(x, y, z) \rightarrow (-x, -y, -z)$. Hence the conditions $x = y = z = 0$ define an invariant subspace \mathcal{M}_s : one initial condition that belongs to this subspace generates a trajectory in phase space that remains in \mathcal{M}_s for any time. This three-dimensional subspace defines the complete (or global) synchronization manifold characterized by $x_1 = x_2$, $y_1 = y_2$, $z_1 = z_2$.

The dynamics in the invariant subspace \mathcal{M}_s , described by the variables (X, Y, Z) , is governed by the equations of the uncoupled Lorenz system, hence there is a chaotic attractor \mathcal{A}_s embedded in \mathcal{M}_s .

Analogously, due to the symmetry $(X, Y, z) \rightarrow (-X, -Y, -z)$, the states for which $X = Y = z = 0$ define another invariant subspace \mathcal{M}_a , associated to a global antisynchronization attractor \mathcal{A}_a , in which (x, y, Z) follows the dynamics of the uncoupled system, i.e. \mathcal{A}_a is likewise a chaotic attractor.

There are also other symmetries in the coupled Lorenz system. For instance, notice in Eqs. (2) that either $(x_1, y_1) \rightarrow (-x_1, -y_1)$ or $(x_2, y_2) \rightarrow (-x_2, -y_2)$ lead, in principle, to the four-dimensional invariant subspaces \mathcal{M}_c and \mathcal{M}_d , respectively. However, these manifolds are not of interest to our analysis, for the parameter intervals and phase space regions considered. We did not find any other relevant coexisting attractor besides \mathcal{A}_s and \mathcal{A}_a .

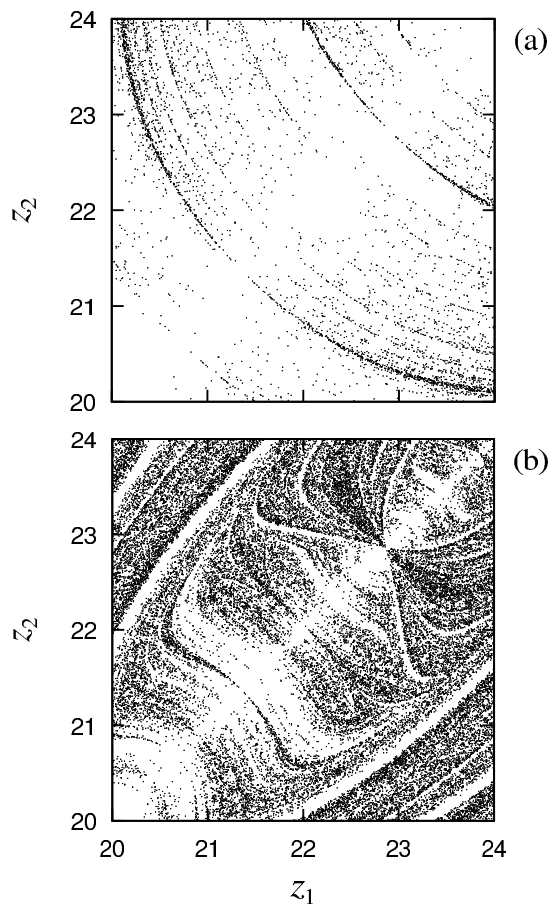


FIG. 1: Section at $x_1 = x_2 = y_1 = y_2 = 1$ of the basins of synchronization (white pixels) and antisynchronization (black pixels) attractors of the coupled Lorenz system, for (a) $\varepsilon = 1.0$; (b) $\varepsilon = 2.0$.

III. BASINS OF ATTRACTION

In dynamical systems with more than one attractor, the corresponding basins may have fractal boundaries and even more complicated structures like the Wada property [18]. Accordingly, in the coupled Lorenz system (2), the two coexisting attractors representing synchronized and antisynchronized states are expected to have such complex basin boundary structure.

Since the phase space of the coupled system is six-dimensional, the visualization of the basins of attraction depends on convenient phase space sections or projections. Figure 1 shows a section of the basin of the antisynchronization (synchronization) attractor \mathcal{A}_a (\mathcal{A}_s). We considered 10^5 initial conditions with $x_1 = x_2 = y_1 = y_2 = 1$ while z_1 and z_2 were randomly chosen in the interval $[20, 24]$ according to a uniform probability distribution.

Each initial condition was integrated using a fourth-order Runge-Kutta scheme with fixed timestep 10^{-3} and for a time 10^3 , after which we determined to what attractor the corresponding orbit has asymptoted. If the orbit has asymptoted to an antisynchronized (synchronized) state in \mathcal{M}_a (\mathcal{M}_s), its initial condition was painted black (white). Hence the area painted black (white) is a numerical approximation of a section of the basin of attractor \mathcal{A}_a (\mathcal{A}_s).

For a coupling strength $\varepsilon = 1.0$ [Fig. 1(a)], the section of the basin of attractor \mathcal{A}_a is a series of thin filaments stemming from the diagonal, whereas “most” of the region is filled with points belonging to the basin of \mathcal{A}_s . The black filaments are non-uniformly distributed and have a suggestive self-similar appearance. In fact, successive magnifications of [Fig. 1(a)] would reveal similar patterns. As another example, for $\varepsilon = 2.0$ [Fig. 1(b)], a similar scenario is observed, but the area occupied by the basin of \mathcal{A}_a has increased, with a corresponding decrease of the basin of \mathcal{A}_s .

As a matter of fact, the structure of the basins of attraction is expected to change with the coupling strength. As an example, in Fig. 2 we show that, for a given value of ε , the same initial condition (given by $x_1 = y_1 = z_1 = 1.0$ and $x_2 = y_2 = z_2 = 0.5$) integrated up to time 10^2 gives distinct trajectories for each system, while for a larger coupling strength the same initial condition produces a single trajectory due to synchronization.

Moreover, the observation of synchronized or antisynchronized states depends on the coupling strength. Let us recall that the existence of \mathcal{M}_s (i.e. the synchronized state being a possible solution of the coupled equations) does not mean necessarily that synchronized states, and in particular states in its embedded attractor \mathcal{A}_s , can be observed in numerical simulations. This occurs only if \mathcal{A}_s is transversely stable, in the sense that any infinitesimal displacement along directions transversal to \mathcal{M}_s decays exponentially with time. Due to the symmetry of the equations with respect to synchronized/antisynchronized states, what holds for attractor \mathcal{A}_s is also valid for \mathcal{A}_a .

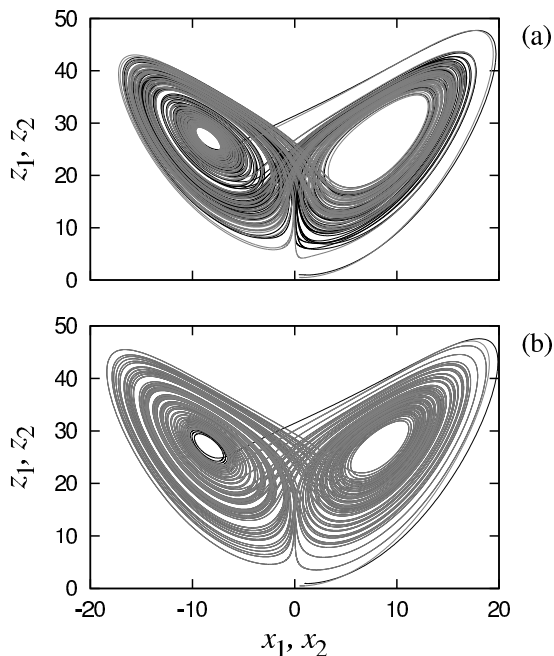


FIG. 2: Attractors of the coupled Lorenz system for the same initial condition, for different coupling values: (a) $\varepsilon = 0.4$; (b) 1.0.

In order to verify the existence of a transversely stable synchronization manifold, we consider the differences $x_1 - x_2$, $y_1 - y_2$, and $z_1 - z_2$, which must vanish if a synchronized attractor is achieved. For $\varepsilon \geq \varepsilon_c \approx 0.75$, $z_1 - z_2$ vanishes at time $t = 10^3$ [Fig. 3(c)], while the other two differences may also vanish (global synchronization) or not (local synchronization) [Fig. 3(a) and (b)]. Similar plots are obtained for the sums $x_1 + x_2$, $y_1 + y_2$, indicating that the basins of the synchronized and antisynchronized states are complementary to each other.

We did not find any attractor for the coupled system other than \mathcal{A}_s and \mathcal{A}_a . Besides the symmetry considerations at the end of Sect. II, we performed the following numerical experiment to reach this conclusion: we considered the initial conditions used to plot the sections of \mathcal{A}_s and \mathcal{A}_a in Fig. 1 and, for each time t we computed the fraction of initial conditions that go either to \mathcal{A}_s or \mathcal{A}_a (circles and dots in Fig. 4(a), respectively). The sum of these fractions rapidly approaches 100% (open squares in Fig. 4(a)), meaning that the fraction of initial conditions that do not asymptote to them goes to zero (filled squares in Fig. 4(a)), suggesting the existence of only two attractors for the coupled system. This conclusion has been observed to hold for $\varepsilon \gtrsim 0.75$ as illustrated in [Fig. 4(b)]. Otherwise, neither synchronized nor antisynchronized states are attained as final ones.

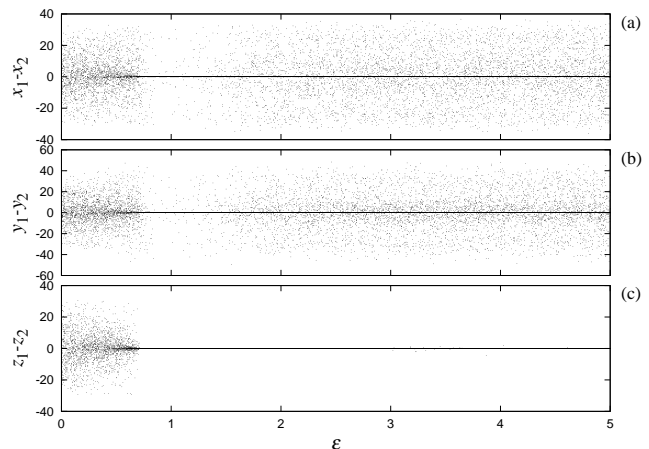


FIG. 3: Difference between the coordinates (a) $x_1 - x_2$; (b) $y_1 - y_2$; (c) $z_1 - z_2$ of two coupled Lorenz systems at time $t = 10^3$, as a function of the coupling strength. One hundred initial conditions were randomly chosen (as in Fig. 1) for each value of ε (varied in steps of 0.01).

IV. RIDDLED AND INTERMINGLED BASINS

Chaotic attractors may have basins riddled with (measure-theoretic) holes belonging to the basin of another attractor [4, 6]. Two basins are said to be intermingled if one basin riddles the other and *vice versa*. The existence of intermingled basins affects our ability of predicting what attractor the trajectory originating from a given initial condition asymptotes to. Let \mathbf{p} be an arbitrary point belonging to the basin of the chaotic attractor \mathcal{A}_a (the same observations holding for \mathcal{A}_s). If the basin of \mathcal{A}_a is riddled by the basin of \mathcal{A}_s , then a small ball of radius ξ and centered at \mathbf{p} has a nonzero fraction of its volume belonging to the basin of \mathcal{A}_s , irrespective of how small the radius ξ might be. Then, the probability that the trajectory will fall into the basin of the other attractor is non-null for every uncertainty ξ . Consequently, riddling is an extreme form of final-state sensitivity.

The existence of intermingled basins implies the fulfillment of the following set of conditions [9]

1. There are invariant subspaces \mathcal{M}_s and \mathcal{M}_a embedded in the system phase space \mathcal{H} ;
2. The dynamics on the invariant subspaces \mathcal{M}_s and \mathcal{M}_a have chaotic attractors \mathcal{A}_s and \mathcal{A}_a , respectively;
3. The attractors \mathcal{A}_s and \mathcal{A}_a are transversely stable in phase space;
4. There are transversely unstable sets of periodic orbits embedded in the chaotic attractors \mathcal{A}_s and \mathcal{A}_a .

In the previous Section we showed that conditions 1 and 2 are fulfilled for the coupled Lorenz systems, no

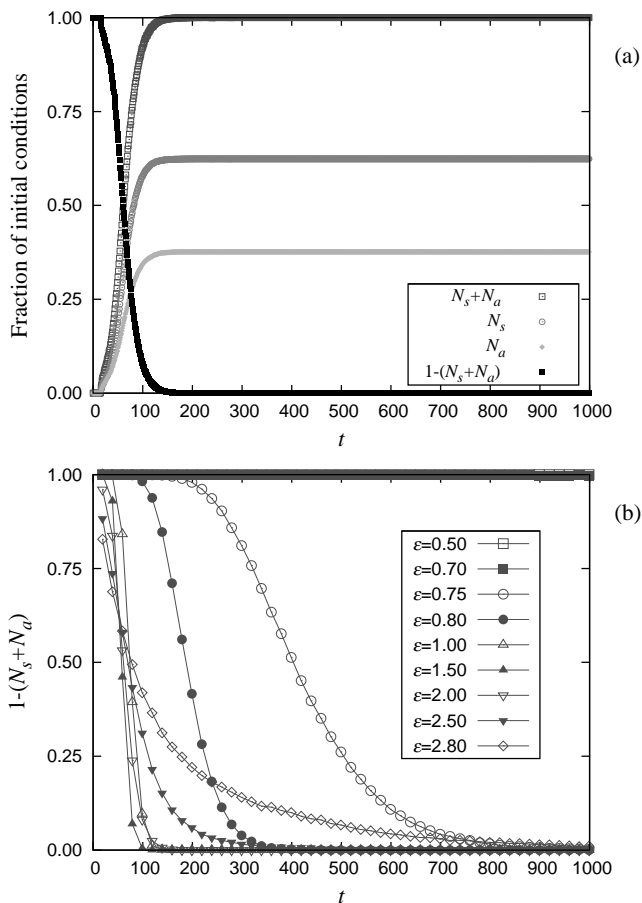


FIG. 4: (a) Fraction of initial conditions yielding trajectories asymptoting synchronized N_s or antisynchronized N_a states as a function of time, for $\varepsilon = 2.0$. We also indicated the fraction of trajectories reaching either state ($N_s + N_a$) or none of them ($1 - N_s + N_a$). (b) Fraction of initial conditions not reaching these states for different values of the coupling strength.

other attractors than $\mathcal{A}_{s,a}$ being observed. The synchronized and antisynchronized manifolds $\mathcal{M}_{s,a}$ are three-dimensional and are embedded in the six-dimensional phase space. For each attractor, there are out of three directions transversal to the respective manifolds. Condition 3 means that the transverse Lyapunov exponents of typical orbits lying in the invariant subspaces (\mathcal{M}_a and \mathcal{M}_s) are all negative. Condition 4 states that, while the invariant subspaces $\mathcal{M}_{s,a}$ may be transversely stable, there will be unstable periodic orbits on the attractors $\mathcal{A}_{s,a}$ that are transversely unstable. These conditions can be numerically verified by computing the finite-time transverse Lyapunov exponents.

For the sake of determining the transversal stability it suffices to consider the largest transversal exponent, denoted as λ_{\perp} . Condition 3 (transversal stability of the attractors) implies that $\lambda_{\perp} = \lim_{t \rightarrow \infty} \tilde{\lambda}_{\perp}(\mathbf{x}_0, t) < 0$ for either \mathcal{A}_a or \mathcal{A}_s , where \mathbf{x}_0 is an initial condition on the basin of attraction.

We computed the Lyapunov exponents using two different methods. The Lyapunov spectrum was obtained following the algorithm of Wolf *et al.* [19], with a Gram-Schmidt normalization step of 0.1. We integrated Eqs. (2) using initial conditions given by $x_1 = y_1 = x_2 = y_2 = 1$ and z_1, z_2 were randomly chosen in the interval $[20, 24)$ from a uniform probability function, as in Fig. 1. These initial conditions lead to trajectories that asymptote to either \mathcal{A}_s or \mathcal{A}_a . As a matter of fact, this is not relevant since both attractors have the same Lyapunov spectrum.

The second method we used, and which can be applied to obtain only the maximal transversal exponent, is to consider the time evolution of an infinitesimal displacement along a direction transversal to the synchronized subspace \mathcal{M}_s , which is given by [4],

$$\lambda_{\perp} = \lim_{n \rightarrow \infty} \frac{1}{n} \ln \frac{\delta(t)}{\delta(0)}, \quad (5)$$

where $\delta(t) = \sqrt{(\delta x)^2 + (\delta y)^2 + (\delta z)^2}$ is the norm of the transverse displacement, whose evolution is given by the variational equations for (x, y, z) , setting $x = y = z = 0$, i.e.,

$$\begin{aligned} \dot{\delta x} &= \alpha(\delta y - \delta x), \\ \dot{\delta y} &= \beta \delta x - \delta y - X \delta z - Z \delta x, \\ \dot{\delta z} &= -(\gamma + 2\varepsilon) \delta z + X \delta y + Y \delta x, \\ \dot{X} &= \alpha(Y - X), \\ \dot{Y} &= \beta X - Y - XZ, \\ \dot{Z} &= -\gamma Z + XY. \end{aligned} \quad (6)$$

Figure 5 shows (using gray symbols) the three largest (infinite-time) Lyapunov exponents as a function of the coupling strength ε , obtained by means of the algorithm by Wolf *et al.*, and the maximal transversal exponent given by (5) is indicated by a thick black line. One of the

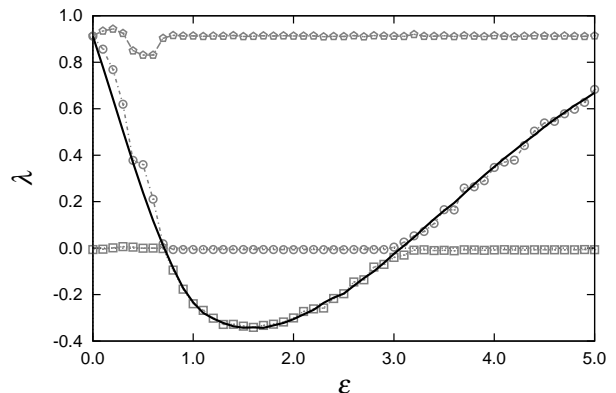


FIG. 5: Variation of the three largest Lyapunov exponents of the coupled Lorenz system as a function of the coupling strength. Gray symbols correspond to the algorithm by Wolf *et al.*, whereas the thick black curve is the result of the variational equations (6).

exponents is always zero, corresponding to displacements along the trajectory. The largest exponent is practically always equal to ~ 0.9 and corresponds to the chaotic dynamics on \mathcal{A}_s (when these computations are performed for initial conditions near \mathcal{A}_a the results are the same). The third exponent is the maximal transversal exponent which we focus our attention on, both methods being in good accord in the region of interest (as shown in Fig. 5). The chaotic attractors in both synchronization and antisynchronization manifolds are transversely stable when the maximal transversal exponent is negative, which corresponds to the interval $\varepsilon_1 < \varepsilon < \varepsilon_2$, where $\varepsilon_1 \approx 0.75$ and $\varepsilon_2 \approx 3.0$, which is also the interval for which condition 3 for intermingled basins is fulfilled.

Finite-time maximal transversal Lyapunov exponents $\tilde{\lambda}_\perp(\mathbf{x}_0, t)$ were computed by means of Eq. (5) but at finite t . Then, for large enough t , one recovers the infinite time exponent λ_\perp , which does not depend on \mathbf{x}_0 , for almost all initial conditions in the attractors $\mathcal{A}_{s,a}$, in contrast to the finite-time ones that may depend on the initial condition.

We quantify the contributions of the finite-time maximal transversal exponent by obtaining a numerical approximation to the corresponding probability distribution function $P(\tilde{\lambda}_\perp(\mathbf{x}_0, t))$. We considered a large number of points in \mathcal{M}_s (with $x = y = z = 0$, $X = Y = 1$, and Z randomly chosen in the interval $[20, 24)$), and discarded a transient to guarantee that the chaotic attractor has been attained. These were the initial conditions to compute the time- t maximal transversal Lyapunov exponents in \mathcal{A}_s . Alternatively, we generated a single long chaotic trajectory (after the transient has elapsed) and divided it into time- t segments, using then the ergodicity of the dynamics to ensure that the conditions are randomly chosen according to the natural measure of the attractor. The results were essentially the same.

Figure 6 shows some probability distribution functions (when $t = 30$) for different values of the coupling strength. In all the considered cases the distribution is nearly Gaussian and presents positive tails.

We can thus verify if condition 4 for riddling is fulfilled by computing the positive fraction of finite-time exponents, $\varphi(t) = \int_0^\infty P(\tilde{\lambda}_\perp(t)) d\tilde{\lambda}_\perp(t) > 0$. The positive fraction as a function of the coupling strength is plotted in Fig. 7 for different values of the time- t interval used to sample the finite-time exponents. We see that results can be strongly dependent on the value of t .

Let us focus our attention first in the case $t = 100$ (represented as diamonds in Fig. 7). For $\varepsilon \lesssim 0.75$ nearly all finite-time exponents are positive. This is consistent with the positivity of the infinite-time exponent shown in Fig. 5 for this region. The positive fraction drops rapidly to 50%, which corresponds to the case for which the infinite-time exponent vanishes, and then drops further to zero, when the infinite-time exponent is negative. As ε increases past ≈ 2.1 the positive fraction takes on nonzero values again and increases until it reaches 50% again for $\varepsilon \gtrsim 3.0$. Comparing with Fig. 5 we see that the

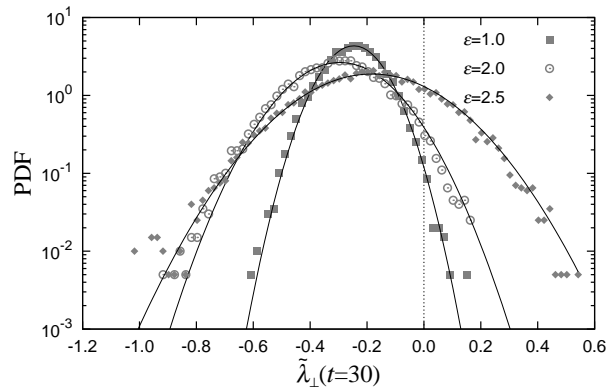


FIG. 6: Probability density functions of the time-30 maximal transversal Lyapunov exponent for different values of ε . Initial conditions were taken as in Fig. 1. The full lines are Gaussian fits.

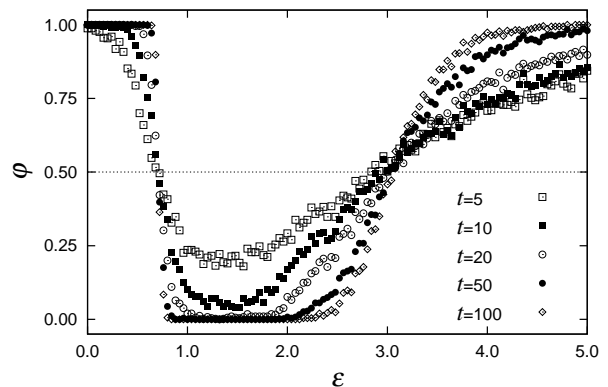


FIG. 7: Positive fraction of the maximal time- t transversal Lyapunov exponent as a function of the coupling strength, for different values of t .

infinite-time exponent is zero at that point. After that, the positive fraction increases gently with ε , yielding a positive infinite-time exponent.

The condition 4 for riddling basins demands the existence of positive fluctuations of $\tilde{\lambda}_\perp(\mathbf{x}_0, t)$, which means a nonzero positive fraction. On the other hand, condition 3 imposes the negativity of the infinite-time exponent λ_\perp . The intersection between the intervals for which both conditions hold simultaneously is a very narrow interval around ~ 0.75 and another interval between 2.1 and 3.0.

Given the dependence on t one may ask how to choose an adequate value for it. There is no simple rule for choosing t , results being dependent on the particular chaotic system being studied. However, we can state a general property: “good” values of t should yield a positive fraction which vanishes when the infinite-time exponent is zero. The reasoning behind this claim is that, for symmetric probability distribution functions (like Gaussian ones), when the distribution maximum is

zero the positive fraction equals 50%: the contribution of the transversely stable periodic orbits embedded in the chaotic attractor is equal to the contribution of the transversely unstable ones. Smaller values of t may not produce good statistics and cannot yield reliable results.

Even within the limitations of this numerical procedure, however, we are able to confirm that the basins depicted in Fig. 1 are indeed intermingled, since the basin of the synchronization attractor riddles the other and *vice versa*.

V. SCALING LAWS FOR INTERMINGLED BASINS

As we have seen in the previous Section, it is sometimes difficult to verify directly the mathematical requirements for riddled and intermingled basins. This is particularly true for high-dimensional systems, like those appearing in many coupled chaotic oscillators. Hence it is important to devise alternative ways to characterize riddled basins, specially when scarce information is available on the high-dimensional dynamics. One such alternative is to verify two scaling laws that hold for riddled basins, which depend on adequate visualization of the basins, as provided by sections like those of Fig. 1.

Let us focus on the black filaments in Fig. 1(b), which belong to the basin of the antisynchronization attractor. They are anchored at the diagonal line, which is a cut of the synchronization manifold \mathcal{M}_s , given by $x = y = z = 0$ and containing a chaotic attractor \mathcal{A}_s , while the antisynchronization attractor \mathcal{A}_a lies elsewhere. In Fig. 8(a) we portrait a schematic picture of that structure. The filaments of the basin of \mathcal{A}_a are tongues anchored at points of \mathcal{A}_s , and the complement of the filament set belongs to the basin of \mathcal{A}_s . If an initial condition starts within any of these narrow tongues, even if it is very close to \mathcal{A}_s , the resulting trajectory will asymptote to \mathcal{A}_a .

The set of basin filaments for \mathcal{A}_a is expected to be self-similar by quite general grounds. The occurrence of riddling is usually triggered by a riddling bifurcation, whereby a periodic orbit embedded in the chaotic attractor of \mathcal{A}_s loses transversal stability and becomes transversely unstable. Once this bifurcation occurs for a given periodic orbit, it also occurs for every preimage of this orbit, yielding a dense set of tongue-like sets anchored at the corresponding preimages on \mathcal{A}_s . The tongue-like shape is a consequence of the nonlinear terms in the equations describing the transversal dynamics. The characteristic feature of riddling is that those tongues have widths that tend to zero as we approach \mathcal{A}_s . Hence the basin of \mathcal{A}_s always contains pieces of basins of \mathcal{A}_a , regardless the transversal distance to \mathcal{A}_s , so forming a fine structure of basin filaments.

This fine structure can be quantitatively characterized by the following numerical experiment [9, 12]: let us consider the invariant manifold at $x = y = z = 0$ and, depart from that manifold, for instance, by increasing z , up to

a distance $l = 2z \equiv z_1 - z_2$ [as depicted by the red line segment in Fig. 8(a)]. Then we evaluate the fraction V_l of points in that segment that belongs to the basin of \mathcal{A}_s . We obtained a numerical approximation of this fraction by considering a number of initial conditions $x = y = 0$, $z = l/2$, $X = Y = 1$, and Z randomly chosen in the interval $[20, 24)$. If the trajectories did not synchronize (within a small tolerance) up to a time 10^3 we consider that they asymptote to the antisynchronization attractor \mathcal{A}_a and, accordingly, they do not belong to the basin of \mathcal{A}_s . If the latter is riddled with tongues belonging to the basin of \mathcal{A}_a , for any distance l (no matter how small) there is always a nonzero value of V_l . This fraction tends to zero as $l \rightarrow 0$. The fraction of length belonging to

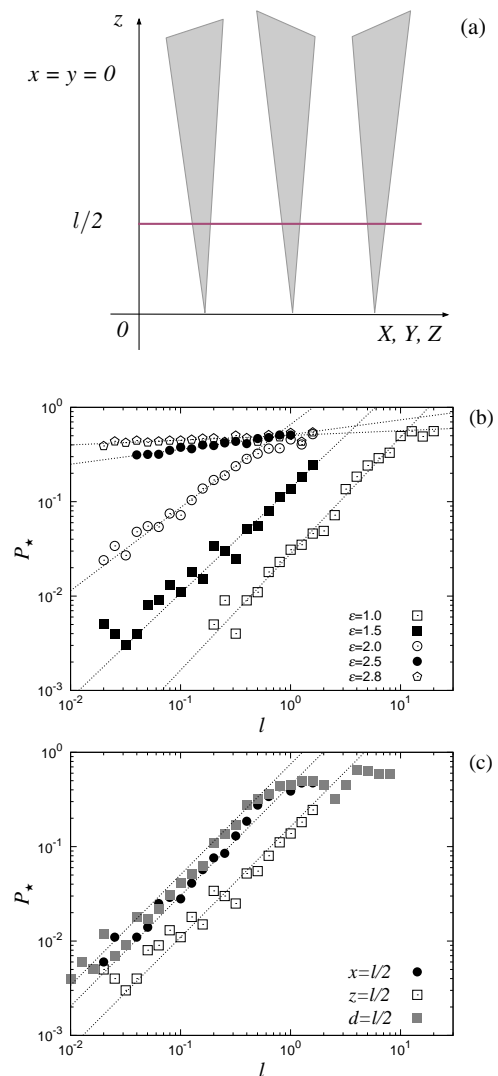


FIG. 8: (a) Schematic figure showing the structure of riddled basins near the invariant subspace that contains a chaotic attractor. (b) Fraction of trajectories P_* that asymptote to the antisynchronized state as a function of the distance $l = 2z$ to the synchronized state, for different values of the coupling strength ε . The full lines are least squares fits. (c) P_* for $\varepsilon = 1.5$ and different definitions of the distance l .

the basin of \mathcal{A}_a can be written as $P_\star = 1 - V_l$, and is expected to scale with l as a power law $P_\star(l) \sim l^\eta$, where $\eta > 0$ is a scaling exponent.

We can regard this scaling law as being related to the fraction of trajectories that do not synchronize. We integrated several initial conditions at the same distance l to the synchronization subspace and computed the fraction P_\star of initial conditions that do not synchronize up to a time 10^3 , repeating this procedure varying the distance l . The results shown in Fig. 8(b) confirm the existence of a power law for this fraction, for many values of the coupling strength.

The results do not vary appreciably when one departs from the synchronization manifold in other directions other than z . In Fig. 8(c) we plotted, for the same coupling strength, the fraction P_\star for initial conditions with $z = l/2$, $x = y = 0$ (open squares), and also for $x = l/2$, $y = z = 0$ (filled circles) and random values of x, y, z such that $d \equiv \sqrt{x^2 + y^2 + z^2} = l/2$ (filled squares), obtaining essentially the same scaling exponent. The dependence of the numerically determined scaling exponents η on the coupling strength is depicted in Fig. 9.

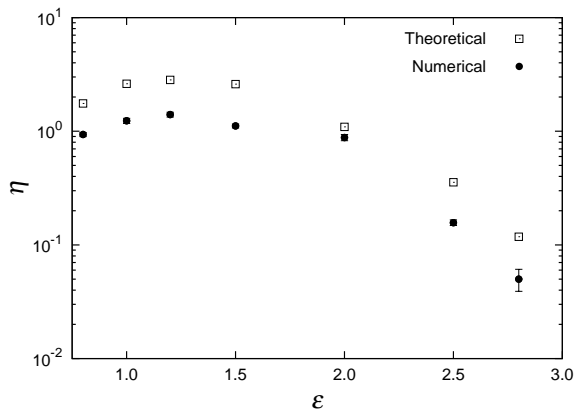


FIG. 9: Scaling exponent η for the fraction of trajectories that asymptote to the antisynchronized state obtained by a numerical experiment (filled circles). For comparison, the theoretical values, given by $\eta = |\lambda_\perp|/D$ are also plotted (open squares).

Another quantitative characterization of riddled basins is based on the uncertain fraction of initial conditions, with respect to their final-state. We may regard riddled basins as an extreme case of fractal basins, for which there is final-state sensitivity and the uncertain fraction of initial condition scales as a power-law with the uncertainty level, whose exponent gives a measure of the extreme final-state sensitivity due to riddling. Consider again the points at $x = y = 0$ and $z = l/2$ drawn in the phase space portrait in Fig. 10(a), as described earlier, and choose randomly an initial condition \mathbf{x}_0 on that region. Now choose randomly another initial condition \mathbf{x}'_0 with uniform probability within an interval of length 2ξ and centered at \mathbf{x}_0 [Fig. 10(a)]. If both points belong

to different basins, they can be referred to as ξ -uncertain [20, 21].

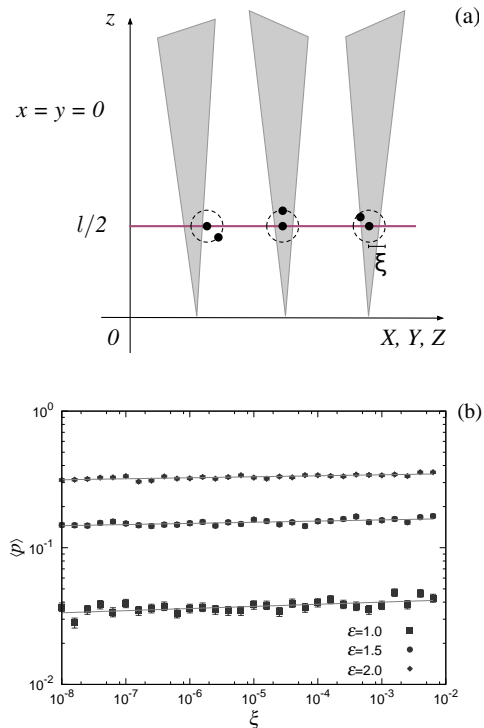


FIG. 10: (a) Schematic figure showing the numerical determination of the uncertain fraction of initial conditions. (b) Uncertain fraction of the initial conditions as a function of the uncertainty level, for different values of the coupling strength. The solid lines are least squares fits.

The fraction of ξ -uncertain points, or uncertain fraction, denoted by $\langle p \rangle$, is the probability of making a mistake when attempting to predict which basin the initial condition belongs to, given a measurement uncertainty ξ . This probability scales with the uncertainty level as a power law of the form $\langle p \rangle \sim \xi^\phi$, where $\phi \geq 0$ depends on both \mathbf{x}_0 and l . For riddled basins, this exponent should be rigorously zero (i.e. there would be no way to decrease the uncertain fraction by decreasing the uncertainty level). Indeed, our results [Fig. 10(b)] support this scaling law, with numerically obtained exponents close to zero.

A stochastic model was proposed by Ott and coworkers to predict the values of the exponents for the two scaling laws we have observed. This model considers the finite-time maximal transversal Lyapunov exponents as random innovations [12]. These exponents are correlated through the deterministic chaotic process governing the system dynamics, which is, in our case the coupled Lorenz equations (2). Nevertheless, if the correlation time is small enough we can treat, in an approximate way, the finite-time Lyapunov exponents $\tilde{\lambda}_\perp(\mathbf{x}_0, t)$ as statistically independent innovations.

An indicator that the correlations in $\tilde{\lambda}_\perp(t)$ fall quickly

to zero, so validating the stochastic approach of Ott *et al.*, is the fact that, by the central limit theorem, the probability distribution function of independent random innovations is Gaussian. The distributions depicted in Fig. 6 confirm the hypothesis that our numerically obtained probability distribution functions $P(\tilde{\lambda}_\perp(t))$ are indeed Gaussian, which improves with larger time- t interval. Accordingly, the variance of this distribution function $\sigma_{\lambda(t)}^2$ is expected to obey a normal diffusive process, i.e. to decay with time as $\sigma_{\lambda(t)}^2 \sim 2D/t$, where D is the corresponding diffusion coefficient.

In order to numerically verify these claims, we plot in Fig. 11 the variance of the probability distribution functions for $\tilde{\lambda}_\perp(t)$ as a function of time, for different values of the coupling strength. The variance decays with time following asymptotically a power-law with exponent -1 , as required for Gaussian diffusion processes.

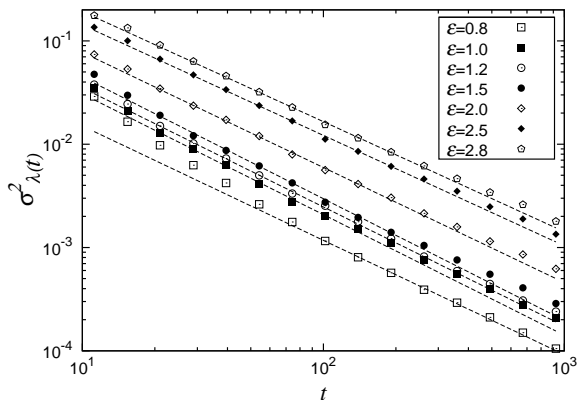


FIG. 11: Time decay of the variance of the finite-time maximal transversal Lyapunov exponent for different values of the coupling strength ε . The lines are least squares fits of the function $f(t) = 2D/t$ to the numerical points, for large t , allowing to estimate the diffusion coefficient D .

This result enables us to model the stochastic dynamics of finite-time (maximum transversal) Lyapunov exponents as a biased random walk described by a Fokker-Planck equation for a probability distribution function. We consider the stationary solution of the stochastic equation, with reflecting boundary conditions at $z = 0$, which predicts a power-law scaling for $P_\star \sim l^\eta$, where the exponent is given by $\eta = |\lambda_\perp|/D$.

The numerical values of η obtained for various values of ε are summarized in Fig. 9. These values are different from those predicted by the biased random walk theory, as also observed for other systems [22]. This discrepancy could be due to prevalence of the correlations caused by the deterministic (chaotic) dynamics. In any case, P_\star displays a power-law decay with l , in accord with the stochastic model, and the power-law exponent η varies with ε following the same tendency predicted by the theory.

Concerning the second scaling law giving the uncertain fraction of initial conditions as a function of the

uncertainty level, the stochastic model of Ott *et al.* also predicts a power-law, where the exponent is given in terms of the infinite-time Lyapunov exponents as $\phi = \lambda_\perp^2/(4D\lambda_\parallel)$, where λ_\parallel is now the maximal longitudinal (and infinite-time) Lyapunov exponent computed for trajectories along the synchronization attractor \mathcal{A}_s . While the theoretical model predicts very small (though nonzero) values, our numerical results for ϕ point out a vanishing result, with negligible numerical fluctuations.

VI. CONCLUSIONS

The Lorenz system is often quoted as a paradigmatic system in nonlinear dynamics, since it displays many interesting dynamical properties of chaotic dissipative systems. Moreover it describes a number of systems of physical interest, like waterwheels, lasers and dynamos. Coupled Lorenz systems could arise as well in the mathematical analysis of related physical problems, in which the spatial extension takes part. The simplest problem in the latter category would be the coupling of two identical Lorenz systems.

Synchronization of chaos in this system, besides its own interest as a mathematical problem, could also be employed in secure communications. We can use the chaotic nature of the dynamics of one of the systems to code messages which could be sent to an identical system through some form of coupling. If the latter system is synchronized with the former, the message can be securely un-coded. The existence of another, antisynchronized state is, in principle, a source of troubles since, depending on the initial condition the receiver system could be tuned to the antisynchronized attractor. Hence it would be necessary here to ensure that a given initial condition will asymptote to the synchronized or the antisynchronized attractor.

The existence of intermingled basins of attraction for the synchronized and antisynchronized chaotic states of this system jeopardizes the solution of that problem, since the initial condition determination is always done within a certain uncertainty level. With intermingled basins, any uncertainty level, however small, lead to complete indeterminacy of the future state of the system. Hence in this case we cannot use synchronization of chaos for any practical purpose, since we will always be haunted by the existence of the another, antisynchronized state, with a basin intermingled with the basin of the synchronized state.

Intermingled basins for the synchronized and antisynchronized attractors of coupled Lorenz systems have been previously suggested in the literature but without a quantitative characterization. In this work we offer numerical evidence that coupled Lorenz systems exhibit intermingled basins of attraction for specified ranges of the coupling parameter. We firstly showed that the mathematical conditions for the existence of intermingled basins are

fulfilled, with the help of properties of finite-time Lyapunov exponents. In a second place, we verified the existence of two scaling laws characterizing quantitatively the degree of uncertainty related to the existence of intermingling basins.

Acknowledgements:

This work was made possible with help of CNPq, CAPES, FAPERJ, and Fundação Araucária (Brazilian

Government Agencies).

-
- [1] M. Bennett, M. F. Schatz, H. Rockwood, and K. Wiesenfeld, Proc. R. Soc. Lond. A **458**, 563 (2002).
 - [2] H. Fujisaka, T. Yamada, Progr. Theoret. Phys. **69**, 32 (1983); L.M. Pecora, T.L. Carroll, Phys. Rev. Lett. **64**, 821 (1990).
 - [3] A. Pikowsky, M. Rosenblum, and J. Kurths *Synchronization: a Universal Concept in Nonlinear Sciences* (Cambridge: Cambridge University Press, 2003).
 - [4] J. Aguirre, R. L. Viana, and M. A. F. Sanjuán, Rev. Mod. Phys. **81**, 333 (2009).
 - [5] C. Grebogi, E. Ott, and J. A. Yorke, Physica D **7**, 181 (1983).
 - [6] J. C. Alexander, J. A. Yorke, Z. You, and I. Kan, Int. J. Bifur. Chaos **2**, 795 (1992).
 - [7] J. C. Sommerer, Apl. Tech. Dig. **16**, 333 (1995).
 - [8] R. F. Pereira, S. Camargo, S. E. de S. Pinto, S. R. Lopes, and R. L. Viana, Phys. Rev. E **78**, 056214 (2008).
 - [9] E. Ott and J. C. Sommerer, Phys. Lett. A **188**, 39 (1994).
 - [10] C.-M. Kim, S. Rim, W.-K. Kye, J.-W. Ryu, and Y.-J. Park, Phys. Lett. A **320**, 39 (2003).
 - [11] M. C. Vergés, R. F. Pereira, S. R. Lopes, R. L. Viana, and T. Kapitaniak, Physica A **388**, 2515 (2009).
 - [12] E. Ott, J. C. Alexander, I. Kan, J. C. Sommerer, and J. A. Yorke, Physica D **76**, 384 (1994).
 - [13] S. Camargo, S. R. Lopes and R. L. Viana, J. Phys. Conf. Series **246**, 012001 (2010).
 - [14] E. N. Lorenz, J. Atmosph. Sci. **20**, 130 (1963).
 - [15] H. Haken, Phys. Lett. A **53**, 77 (1975).
 - [16] E. Knobloch, Phys. Lett. A **82**, 439 (1981).
 - [17] R. Karnatak, R. Ramaswamy, and A. Prasad, Phys. Rev. E **76**, 035201 (2007).
 - [18] H. E. Nusse, J. A. Yorke, Science **271**, 1376 (1996).
 - [19] A. Wolf, J. B. Swift, H. L. Swinney, and J. A. Vastano, Physica D **16**, 285 (1985).
 - [20] C. Grebogi, S. W. McDonald, E. Ott, and J. A. Yorke, Phys. Lett. A **100** 1 (1985).
 - [21] S. W. McDonald, C. Grebogi, E. Ott, and J. A. Yorke, Physica D **17** 125 (1985).
 - [22] Y.-Ch. Lai and V. Andrade, Phys. Rev. E **64**, 056228 (2001).